

Low Temperature Sensitization on the Orthogonal Surfaces of Prior Deformed AISI 304LN and Aged at 673 K to 873 K (400 °C to 600 °C)

RAGHUVIR SINGH, S. GHOSH CHOWDHURY, GAUTAM DAS, P.K. SINGH,
and I. CHATTORAJ

This study investigates the sensitization behavior of AISI 304LN deformed previously by cold rolling (CR) to 5 pct to 25 pct reduction in thickness and aged at 673 K to 873 K (400 °C to 600 °C). The emphasis was on revealing the degree of sensitization (DOS) resulting from low-temperature sensitization (LTS) on the orthogonal surfaces and correlation thereof with the changes in various metallurgical properties caused by cold rolling. It was found that the DOS differs among the orthogonal surfaces such as the rolling surface (RS), transverse surface (TS), and cross transverse surface (CTS). RS showed lower DOS compared with CTS and TS. The differences in the DOS were attributed to the combined effect of deformation-induced martensite (DIM), grain size, and slip band formation. A deformation of 5 pct was critical to the susceptibility of AISI 304LN to intergranular (IGC) and transgranular corrosion (TGC). The sensitization kinetics was slow or saturated leading to desensitization beyond 5pct deformations at 773 K (500 °C) and 873 K (600 °C). It was, however, uniformly accelerated over 5 to 25 pct deformation when aged at 673 K (400 °C).

DOI: 10.1007/s11661-011-1011-6

© The Minerals, Metals & Materials Society and ASM International 2011

I. INTRODUCTION

LOW temperature sensitization at ≤ 773 K (500 °C) in austenitic stainless steels is extremely relevant to several industrial processes such as in nuclear power plants that use stainless steels and operate at 573 K to 773 K (300 °C to 500 °C).^[1,2] Chromium carbide nucleation in austenitic stainless steels is possible during the fabrication processes such as during welding, thermo-mechanical processing, slow cooling during solution annealing, and stress relief annealing. Such steels may contain carbide nuclei that are not necessarily accompanied by a chromium-depleted zone critical for sensitization-induced failures in corrosive environments. The carbide nuclei may, however, proliferate at operating temperatures < 773 K (500 °C) (below classic sensitization temperature) and broaden the chromium-depleted zone after prolonged service exposure to cause sensitization related failures. This was verified by several failures encountered in the nuclear industries and analysis thereof.^[1-4] At temperatures greater than 773 K (500 °C), sensitization occurs by bulk chromium diffusion (activation energy ~ 265 kJ/mole) and by grain boundary chromium diffusion at low temperatures (activation energy of 100 to 150 kJ/mole).^[3] Thus, prediction of low-temperature sensitization (LTS)

behavior by extrapolating the sensitization data obtained at high temperature may cause wide scatter in the results. LTS in boiling water reactor of nuclear power plants is being reexamined because of several reasons, such as growing demands for longer service life (as high as 100 years) of engineering components and safety issues during long-term plant operation. This has changed the materials-selection strategy to high-performance stainless steels such as 304LN and 316LN in place of 304/304L or 316/316L, which are yet to be investigated in details for their LTS susceptibility.

The kinetics of sensitization in stainless steel is reported to be accelerated by deformation. Deformation in stainless steels may be prevalent from prior processing including fabrication; welding can introduce strains as high as 20 pct in the heat-affected zone of stainless steel. The deformation prior to sensitization decreases the temperature for carbide nucleation and accelerates carbide precipitation at a normal sensitization temperature compared with undeformed stainless steels.^[5-12] In the cold-rolled sheet or plate, a variation of stress/strain, stress state, texture, and microstructures is expected on orthogonal surfaces of a sheet. It is known that certain properties such as yield and tensile strength in the cold-rolled sheet are anisotropic, and component failures are often related to the anisotropic behavior of materials.^[13] A study has shown already that the crevice corrosion resistance differs among the orthogonal surfaces.^[14] It may be, therefore, important to ensure the surface that has to encounter the corrosive environment contains intergranular corrosion (IGC) resistance desirable for the long service life of components. The objective of this study was to investigate the variation of the degree of sensitization (DOS), if any, on three

RAGHUVIR SINGH, S. GHOSH CHOWDHURY, GAUTAM DAS, and I. CHATTORAJ, Scientists, are with the Council of Scientific & Industrial Research-National Metallurgical Laboratory (CSIR-NML), Jamshedpur 831007, India. Contact e-mail: raghujog@yahoo.co.in P.K. SINGH, Scientist, is with the Reactor Safety Division, Bhabha Atomic Research Centre, Mumbai 400 085, India.

Manuscript submitted June 17, 2011.

Article published online November 30, 2011

orthogonal surfaces of thick sections, a subject that is not reported in the literature. The definition of a critical limit on the extent of deformation prior to exposure that does not lead to sensitization is essential for the selection of material and fabrication processes, which was also within the scope of the current study.

II. EXPERIMENTAL DETAILS

Stainless steels 304LN (composition in wt pct: C-0.01 Si-0.31, Mn-0.93, Cr-17.4, Mo-0.18, Ni-11.06, N-0.10,

and Fe-balance) were cut to a $100 \times 25 \times 14$ mm plate from pipe. The plates were solution annealed at 1343 K (1070 °C) for 1 hour followed by water quenching. They were then subjected to cold rolling, resulting in 5 to 25 pct reduction in thickness, with a maximum reduction of 5 pct per rolling pass. The rolled plates were subjected to an aging treatment at 673 K (400 °C), 723 K (450 °C), 773 K (500 °C), and 873 K (600 °C) for 8000, 1280, 264, and 18 hours, respectively, followed by furnace cooling. The durations of aging at various temperatures were worked out to simulate 100 years of exposure at 573 K (300 °C) using an Arrhenius equation

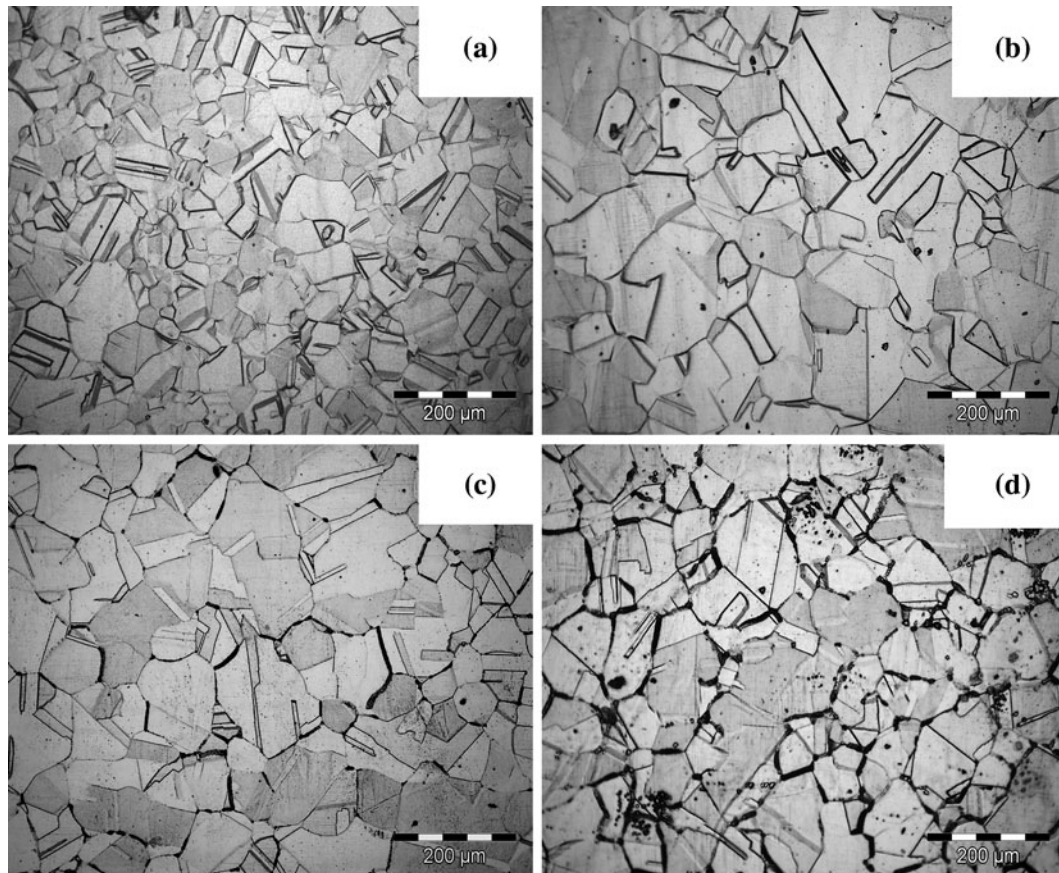


Fig. 1—Microstructure of undeformed (RS) AISI 304LN revealed by EOA etching after sensitization at (a) 673 K (400 °C), (b) 723 K (450 °C) (c) 773 K (500 °C), and (d) 873 K (600 °C).

Table I. Categorization of the Microstructures after EOA Etching

| Percent CR | Aging Temperatures [K (°C)] | | | | | | | | | | | |
|------------|-----------------------------|------|------|-----------|-------|------|-----------|-------|-------|-----------|-------|-------|
| | 673 (400) | | | 723 (450) | | | 773 (500) | | | 873 (600) | | |
| | RS | TS | CTS | RS | TS | CTS | RS | TS | CTS | RS | TS | CTS |
| 0 | step | step | step | step | step | step | dual | step | step | dual | dual | dual |
| 5 | step | step | step | dual | dual | step | ditch | ditch | ditch | ditch | ditch | ditch |
| 10 | step | step | — | dual | dual | dual | ditch | ditch | ditch | ditch | ditch | ditch |
| 15 | dual | dual | dual | dual | dual | dual | ditch | ditch | ditch | ditch | ditch | ditch |
| 20 | dual | — | — | dual | ditch | dual | ditch | ditch | ditch | ditch | ditch | ditch |
| 25 | dual | — | dual | dual | dual | dual | dual | ditch | ditch | dual | ditch | ditch |

as done elsewhere.^[15] Sensitization is considered to be a diffusion-enhanced process for which the Arrhenius rate equation can be used.

After aging, the specimens with dimensions of $15 \times 10 \times t$ (thickness) were cut from the plates, and ground and polished up to 1200 grit emery paper. Cloth polishing was then performed using diamond paste ($\sim 0.5 \mu\text{m}$) followed by degreasing in acetone. The specimens thus polished were used for the detection and evaluation of intergranular corrosion by electrolytic

oxalic acid (EOA) etching according to ASTM A262-A^[16] and double-loop electrochemical potentiokinetic reactivation (DL-EPR) tests. For ASTM A262-practice E tests, the specimens were cut in the size as described by the ASTM standard and polished up to the 600-grit emery paper.

Sensitization was evaluated qualitatively by using standard test methods such as EOA etching and ASTM A 262-practice E, as described elsewhere.^[16] The microstructures obtained after EOA etching were classified as

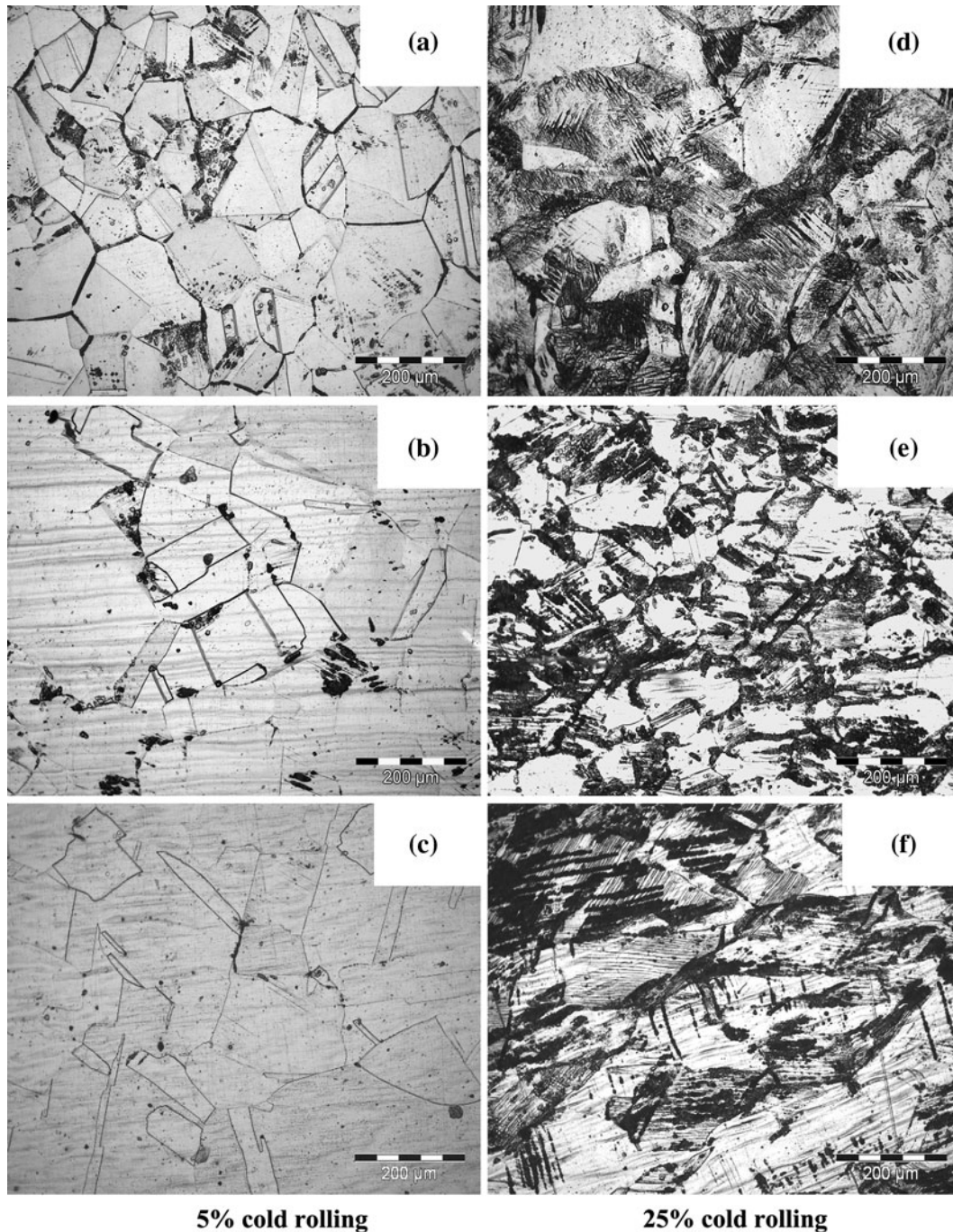


Fig. 2—Microstructures of AISI 304LN sensitized at 723 K (450 °C) after deforming, revealed by EOA etching on RS—(a) and (d); TS—(b) and (e); and CTS—(c) and (f).

step, dual, or ditch according to their grain boundary features. For ASTM A262- practice E, the sensitized specimens were exposed to the boiling copper sulfate and sulfuric acid solution with addition of copper shots for 48 hours. The specimens were then subjected to bending; the bent area was observed under the optical microscope and scanning electron microscope (SEM). Sensitization was determined quantitatively by the DL-EPR method at an ambient temperature as described elsewhere.^[15] The test solution was prepared from

reagent-grade chemicals and made up of 0.5 M H₂SO₄ and 0.01 M KSCN in distilled water. The specimens were polarized anodically from -100 mV with respect to open circuit potential up to +300 mV (with respect to saturated calomel electrode), and then the scan was reversed at a scan rate of 6 V/h. The percent DOS was evaluated by measuring the ratio of $(I_r/I_a) \times 100$, where I_r is the peak reactivation current density and I_a is the peak activation current density. The DL-EPR experiments on each specimen set were repeated for three

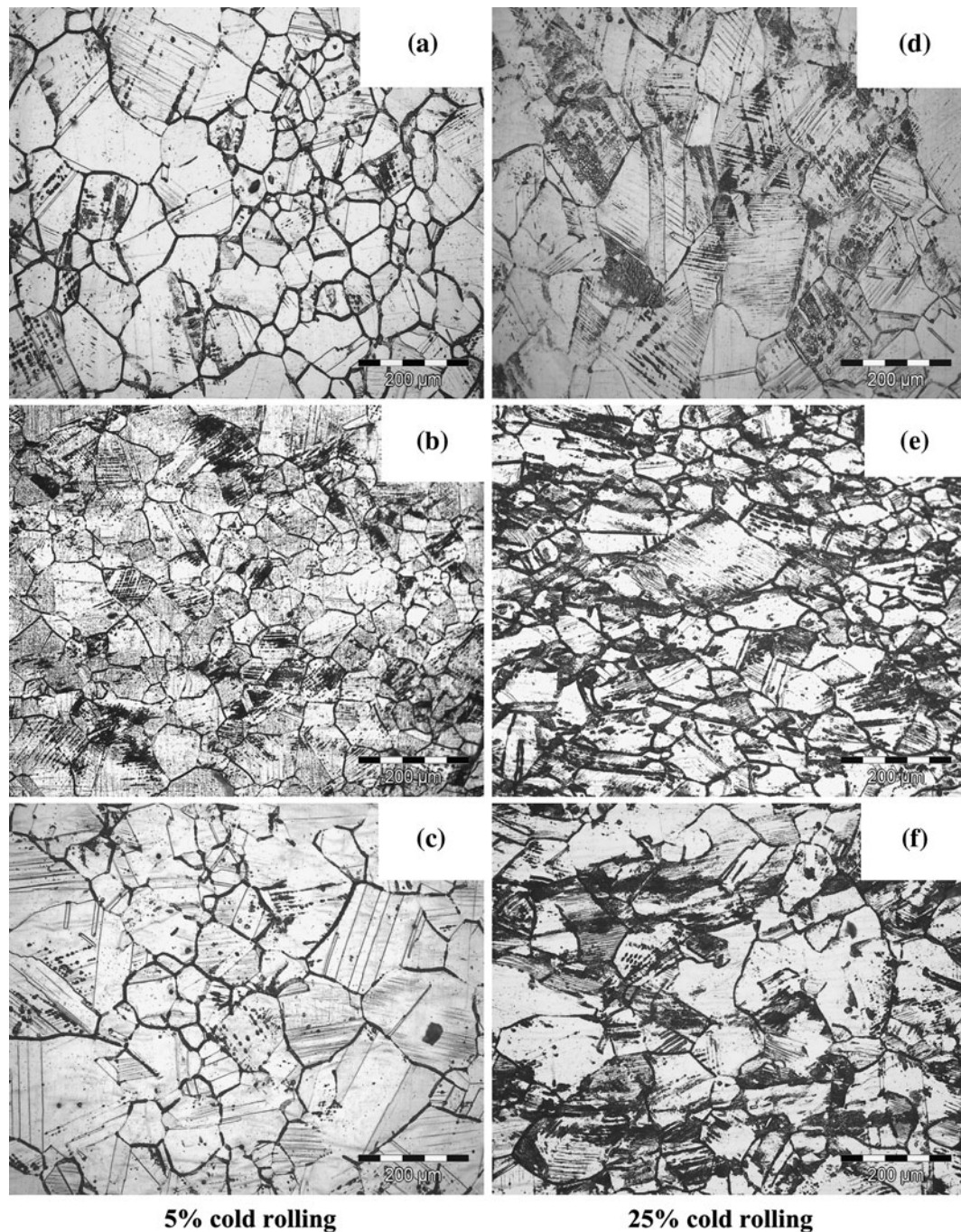


Fig. 3—Microstructures of AISI 304LN sensitized at 773 K (500 °C) after deforming, revealed by EOA etching on RS—(a) and (d); TS—(b) and (e); and CTS—(c) and (f).

times in fresh solution, and the average values are reported. The evaluation of sensitization was made on the orthogonal surfaces namely the rolling, transverse, and cross-transverse surfaces of the specimen.

Deformation-induced martensite (DIM), which was formed during cold rolling, was detected by X-ray diffraction and also by ferrite meter. The texture developed because of cold rolling was measured on the rolled surface of the specimens in an X-ray diffractometer using the Schultz reflection technique. Four incomplete pole figure $\{111\}$, $\{200\}$, $\{220\}$, and $\{113\}$ were measured, and the orientation distribution function (ODF) was evaluated with cubic sample symmetry with arbitrarily defined cells method. Microstructural investigations were carried out on some of the samples with CM 200 transmission electron microscope operated at 200 kV.

III. RESULTS

A. Effects of Deformation on Sensitization

Optical microstructures obtained from EOA etching are illustrated in Figures 1 through 3, and corresponding

microstructural categorization made according to ASTM A262-A^[16] is summarized in Table I.

CR, cold rolling; CTS, cross transverse; RS, rolling surface; TS, transverse surface.

EOA etching of undeformed specimens aged at 673 K (400 °C) and 723 K (450 °C) (TS and CTS) showed “step” microstructure, indicating a nonsensitized state of the stainless steel 304LN (Figures 1(a) and (b)). The undeformed samples aged at 773 K (500 °C) and 873 K (600 °C), however, revealed the “dual” microstructure and, thus, showed the onset of sensitization at this temperature (Figures 1(c) and (d)). A qualitative comparison of microstructures (Figures 2 and 3 and Table I) shows clearly that the deformation prior to aging at 673 K to 873 K (400 °C to 600 °C) resulted in increase in sensitization. An undeformed specimen that did not undergo sensitization and showed step microstructure transformed to “dual,” such as on aging at 673 K (400 °C) and 723 K (450 °C), and “ditch,” such as on aging at 773 K (500 °C) and 873 K (600 °C) after deformation prior to aging. The microstructures of cold-rolled specimens obtained from EOA etching showed the darkening (caused by corrosion) of grain

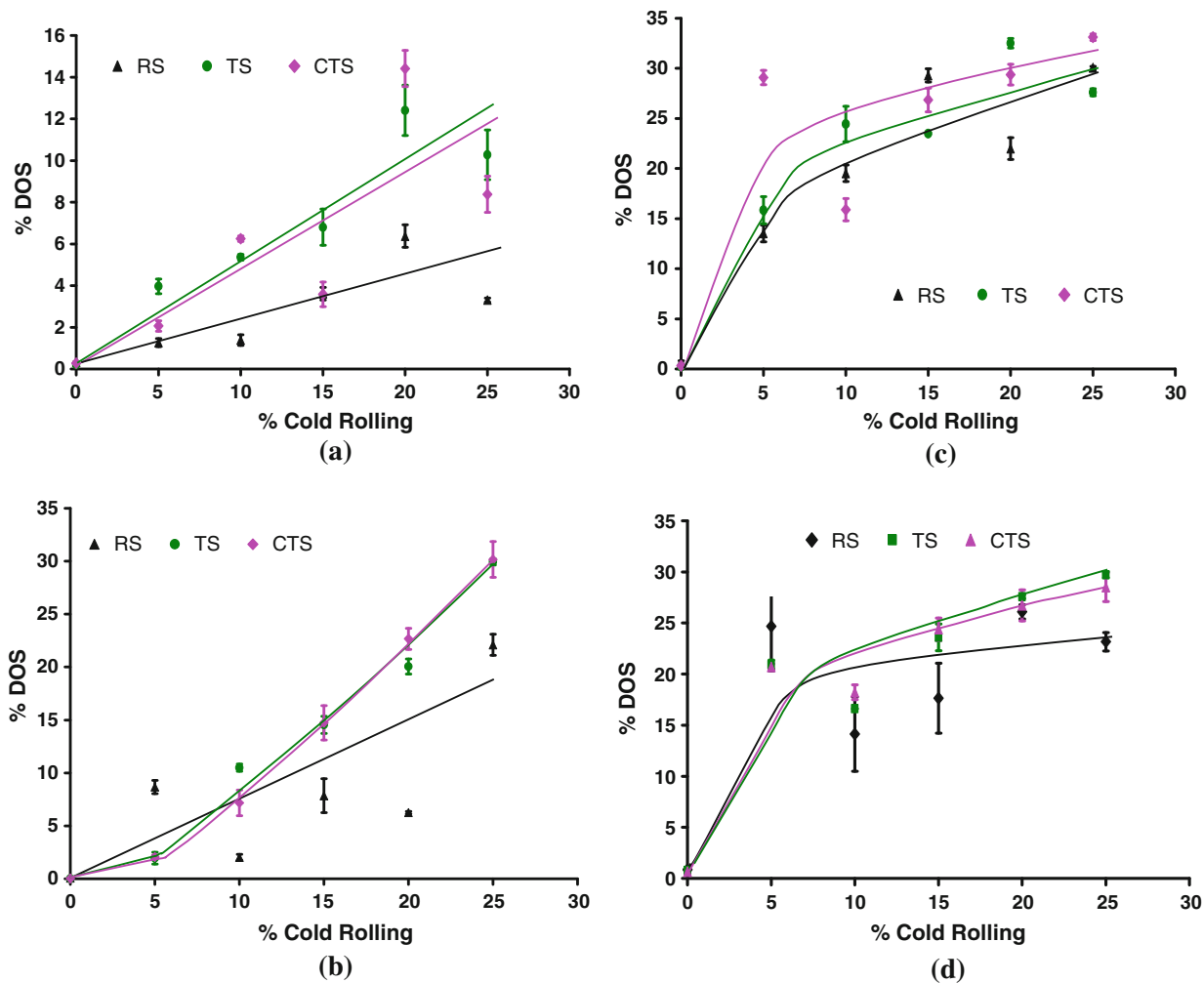


Fig. 4—Variation in the degree of sensitization on RS, TS, and CTS with percent cold rolling after aging at (a) 673 K (400 °C), (b) 723 K (450 °C), (c) 773 K (500 °C), and (d) 873 K (600 °C).

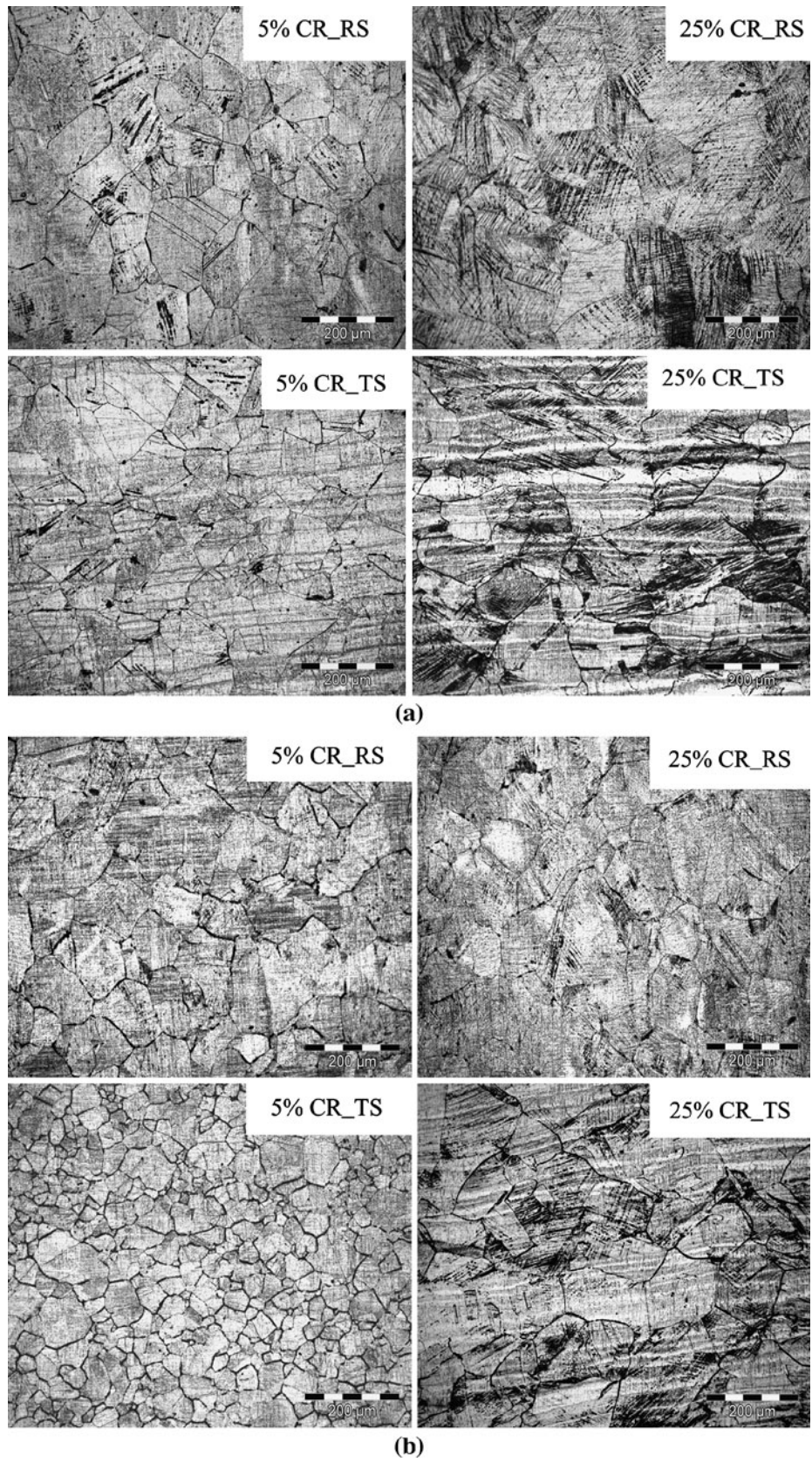


Fig. 5—Post-DL-PR microstructures of specimens aged at (a) 723 K (450 °C) and (b) 873 K (600 °C).

interiors, in addition to grain boundaries (Figures 2 and 3). The corrosion attack in the grain interiors was noticed to increase with percent cold rolling. This fact was confirmed by quantifying the sensitization in terms of degree of sensitization as illustrated in Figures 4(a) through (d). The average DOS values for undeformed 304LN remained lower than 1.0 pct at all the aging temperatures. It may indicate that none of the undeformed 304LN specimens are prone to intergranular stress corrosion cracking (IGSCC). It has been shown that the low-carbon and stabilized stainless steels with DL-EPR values below 1.0 pct were highly resistant to IGSCC in oxygenated high-temperature water.^[17] The slow strain rate tests carried out on 304L stainless steel at even more aggressive conditions also demonstrated no IGSCC below 1 pct DOS by DL-EPR.^[17] Stainless

steel 304L having DOS values ≥ 3 pct were reported to suffer from IGSCC.^[18]

Figures 4(a) through (d) represent the effect of cold rolling on DOS in three orthogonal surfaces. It indicates clearly the increase in DOS with percent rolling from 5 to 25 pct, and it substantiates the observations from EOA etching. The maximum DOS value at 25 pct cold rolling was obtained for specimens aged at 773 K (500 °C) followed by those that were aged at 723 K (450 °C) and 873 K (600 °C). It was the lowest (at 25 pct cold rolling) for a specimen aged at 673 K (400 °C). The specimens aged at 773 K to 873 K (500 °C to 600 °C) showed the highest rate of increase of sensitization below 5 pct deformation, beyond which it slows down as evident from the slopes of DOS versus percent rolling curves shown in Figures 4(c) and (d). The difference in DOS values obtained for

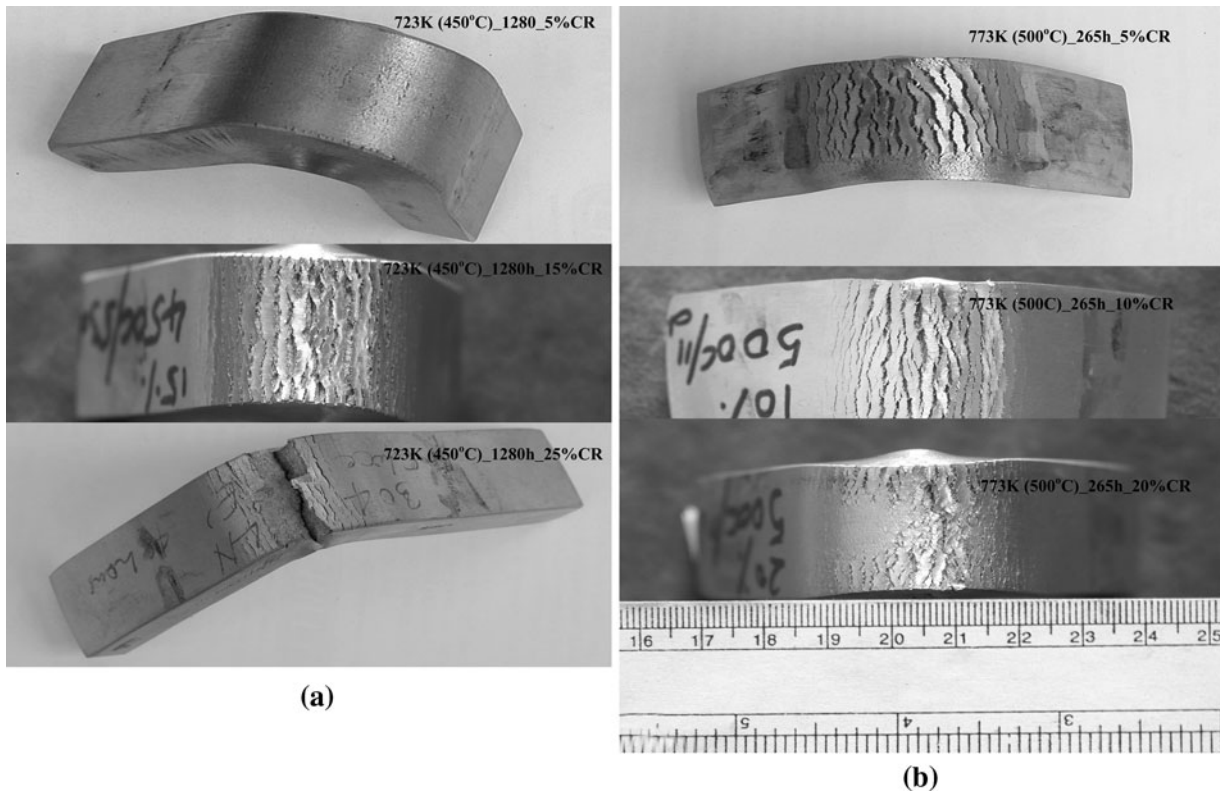


Fig. 6—Photographs showing fissure/cracks on the bent surface after practice E test on specimens sensitized at (a) 723 K (450 °C) and (b) 773 K (500 °C).

Table II. Summary of Results from ASTM A262-Practice E Test

| Percent CR | Aging Temperatures [K (°C)] | | | |
|------------|-----------------------------|-----------------|-----------------|-------------|
| | 673 (400) | 723 (450) | 773 (500) | 873 (600) |
| 0 | no fissures | no fissures | no fissures | no fissures |
| 5 | no fissures | cracks/fissures | cracks | fissures |
| 10 | cracks/fissures | cracks/fissures | cracks | fissures |
| 15 | fissures | cracks/Fissures | cracks | fissures |
| 20 | cracks/fissures | cracks/fissures | cracks | no fissures |
| 25 | cracks/fissures | cracks | cracks/fissures | no fissures |

specimens aged at 723 K (450 °C), 773 K (500 °C), and 873 K (600 °C) were found to decrease with an increase in deformations, which may be due to the result of attaining near saturation in microstructural changes. This might be an indication of onset of desensitization. A large difference in DOS values between specimens aged at 673 K (400 °C) and above shows clearly the temperature effects on variation of sensitization kinetics. At 673 K (400 °C), it has been observed that the DOS values at three orthogonal surfaces differ significantly with an increase in percent cold rolling; the values of percent DOS on RS are lower compared with TS and CTS at cold rolling from 0 to 25 pct. A previous report that considered AISI 304 stainless steel prior deformed at 0 to 80 pct CR followed by aging at 773 K to 973 K (500 °C to 700 °C) showed maximum

DOS at 20 or 40 pct CR at 973 K (700 °C) and 873 K (600 °C).^[10] The specimen aged at 773 K (500 °C), however, did not show such maxima; rather, DOS increased monotonously with cold rolling from 0 to 80 pct.^[10] This is similar to that which is observed at 673 K (400) and 723K (450°C) in the present investigation (Figures 4(a and b)). The post DL-EPR microstructures in Figure 5 revealed significant corrosion inside the grain matrix and along the grain boundaries, as also appeared in the EOA etched microstructures. The corrosion in the interior of the grains is prevalent particularly at the larger deformation levels such as at 25 pct.

The intergranular corrosion was studied by subjecting the sensitized specimens to the more rigorous ASTM A262-practice E test.^[16] On bending the specimens

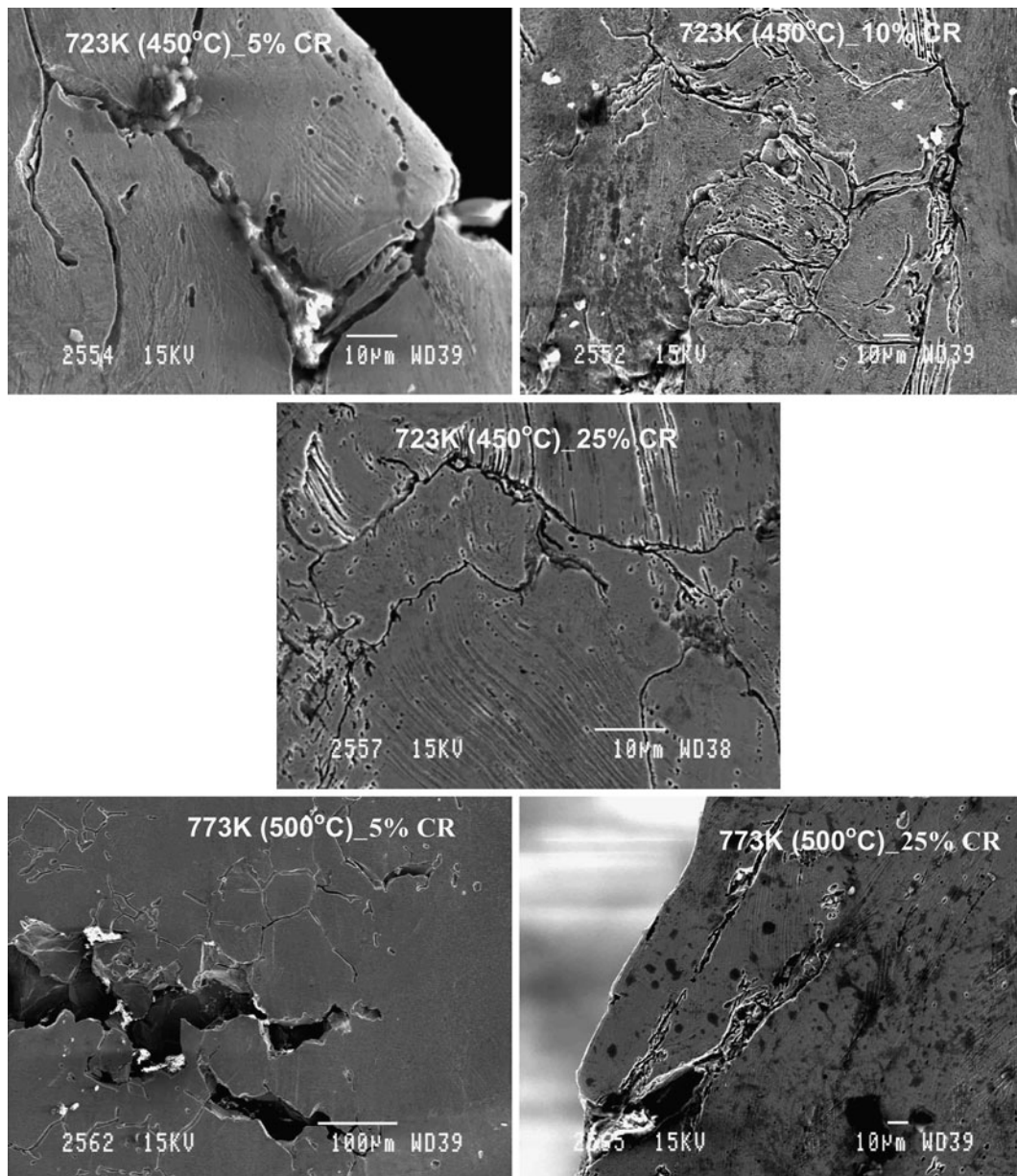


Fig. 7—Fractographs showing the crack propagation in the cross section of specimens aged at 723 K (450 °C) and 773 K (500 °C) after ASTM 262A-practice E test.

subsequent to the boiling in a sulfuric acid–copper sulfate solution, fissures/cracks appeared on several specimens and were visible clearly as illustrated in Figure 6. The RS was bent for all the specimens during the ASTM A262-practice E test. In general, the bent surface was observed to have either no fissures (passing the test for IGC) or mild fissures, or severe cracks (failing the IGC test according to ASTM Standard). Undeformed specimens, aged at all conditions, did not result into fissures/cracks, whereas most of those that were rolled prior to aging showed fissures/cracks on the bent region (Figure 6). These results are summarized in Table II.

Specimens that have undergone severe cracking are mentioned as “cracks,” and those that contained mild fissures along with significant cracks are indicated as “fissures/cracks” in the table. Fissures are mentioned only for mild fissures without significant cracks. The ASTM standard,^[16] however, does not discriminate between mild fissures or severe cracks. Visually, of all the specimens, those that were aged at 773 K (500 °C) showed relatively more severe cracks followed by those aged at 723 K (450 °C). Aging at 873 K (600 °C) showed mild or no fissures on the surface. Generally, such an IGC test (ASTM A262-practice E) is applicable to the undeformed specimens as severe cold rolling reduces the ductility of stainless steels and might result in cracking on the strained regions on bending (even without sensitization). The specimens cold rolled (up to 25 pct) without sensitization were bent (from rolling surface) similarly as done after the IGC exposure. None of these have experienced fissures/cracks on the bent zone. Cross sections (perpendicular to fissures/cracks) were investigated under the SEM to understand whether cracks follow a preferential path of failure. A few such micrographs are given in Figure 7 to show the crack path along the thickness of the specimens. The observations under SEM were made on outermost (near) surface of the bent zone that had encountered IGC during the boiling test. The corrosion cracks in the specimen rolled to 5 pct deformation were found to

follow an intergranular path, but for higher deformations, cracks propagated in a mixed mode (intergranular and transgranular) as shown in Figure 7. This was also confirmed by observing the cross section of specimens treated in boiling solutions of ASTM A262-practice E but without bending. Such optical micrographs of 5 and 25 pct cold-rolled samples are presented in Figure 8. Corrosion took place, apparently in 5 pct cold rolled specimens (in Figure 8), approximately one grain layer deep along the grain boundary from the surface. However, no such preference of corrosion along grain boundaries was observed in the specimens rolled beyond 5 pct (such as 25 pct cold-rolled sample in Figure 8). It might thus be inferred that 5 pct cold rolling is a critical deformation level in 304LN, beyond which an IGC mechanism shifts from a purely intergranular to a mixed mode. The crack propagation path here does not necessarily mirror what is observed typically in the specimens failed during stress corrosion cracking or IGSCC test. The bending opens up the regions that had undergone intergranular or intragranular corrosion during boiling

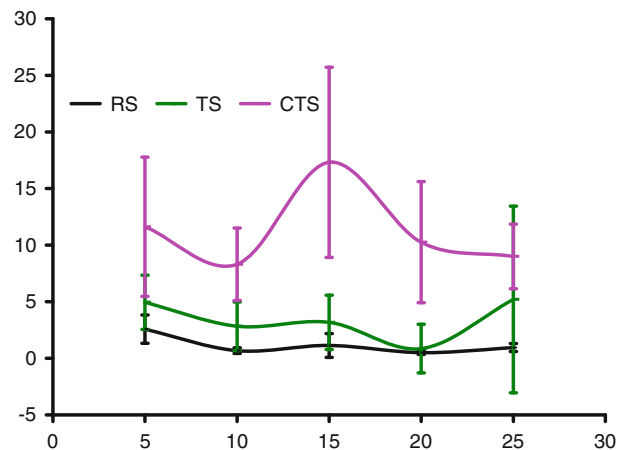


Fig. 9—Quantification of martensite phase along RS, TS, and CTS.

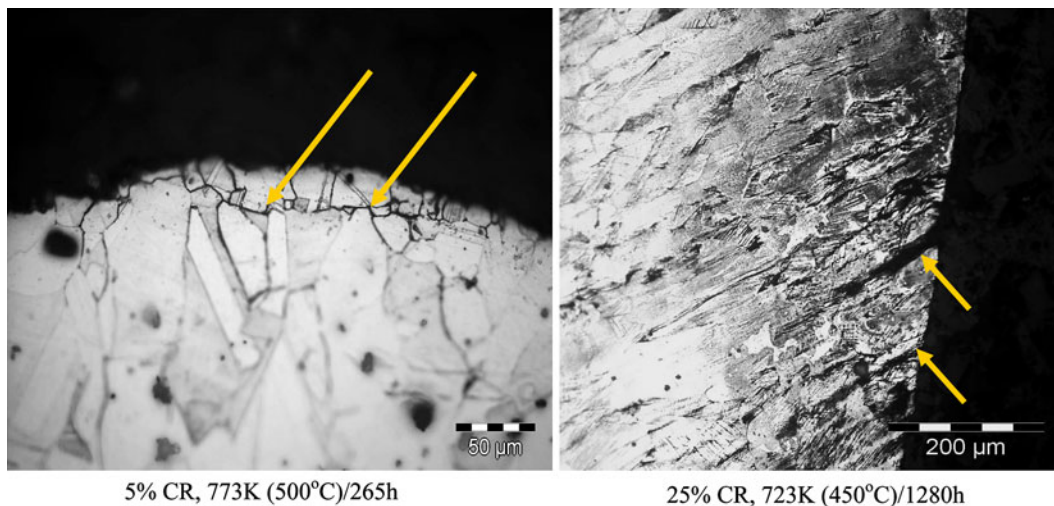


Fig. 8—Intergranular corrosion propagation after boiling in solution of ASTM A262-practice E.

in sulfuric acid–copper sulfate solution. Any intergranular or transgranular cracking in the current investigation indicates the presence of chromium-depleted zones, which were corroded preferentially during the subsequent tests.

The acceleration of sensitization at 673 K to 873 K (400 °C to 600 °C), in specimens with prior deformation, is possibly caused by several changes affecting the kinetics of carbide precipitation, and proliferation of carbides, such as changes in activation energy, microstructure, phase, *etc.* in the base stainless steel brought about by deformation. Reportedly, deformation (by ~20 pct) reduces the activation energy of stainless steel AISI 304 by 22.9 Kcal/mol and of AISI 316 by approximately 14 Kcal/mol.^[19] The decrease of activation energy facilitates carbide precipitation by enhancing chromium diffusion through “dislocation pipes.” The defects and dislocations introduced by deformations are the preferred sites for carbide precipitation. The dislocation density in solution-annealed stainless steel 304 has been shown to increase by approximately two orders (up to $6 \times 10^{10}/\text{cm}^2$) after 25 pct cold rolling.^[20] Also, stainless steel 304 is prone to phase change from austenite to martensite on cold deformation.^[21,22] Deformation-induced martensite (DIM) with its body-centered cubic (bcc) structure is more favorable for carbon and chromium diffusion than the austenite phase (face-centered cubic). In the current study, martensite was detected and quantified in 304LN (having $M_{d30} \sim 9.7$ °C), with respect to percent cold rolling along three orthogonal surfaces as shown in Figure 9. It shows that the DIM did not vary significantly with an increase in cold rolling up to 25 pct. The DIM determined along the rolling direction by the ferrite meter showed the ferrite numbers ranging from 0.14 to 0.46 at 5 to 25 pct, respectively. It persists even after aging the cold-rolled specimens at 673 K to 773 K (400 °C to 500 °C). Similar observations indicating no change in DIM (in 304 and 304L) up to 773 K (500 °C) and deformed by approximately 50 pct after heat treating at 823 K (550 °C) were reported.^[22] An increase in DOS with cold rolling may thus be related to the changes caused by the deformation, such as an increase in dislocation density, lowering of activation energy, and evolution of DIM phase. It is apparent from Figure 4 that the kinetics of sensitization are different for deformations above and below 5 pct and is temperature dependent. At 773 K to 873 K

(500 °C to 600 °C), the increase in sensitization is large at initial deformations (<5 pct), whereas at 723 K (450 °C), it is found to be greater beyond 5 pct deformation for TS and CTS. It seems that at 773 K (500 °C) and 873 K (600 °C), DOS reaches saturated values and subsequent deformation does not increase it significantly, *i.e.*, in a manner such as at <5 pct deformation. It possibly follows the increasing trend of dislocations with pct deformations. This is evident from the variation of hardness with increasing deformations as presented in Table III.

The hardness of the solution-annealed stainless steel was observed to increase by ~34 pct (117 Hv) on applying 25 pct deformation, out of which an 18 pct (64 Hv)

Table III. Variation in Hardness with Increase in Deformations

| Percent Cold Rolling | Hardness, HV _{100g} (Maximum Deviation) | | |
|----------------------|---|-----------|-----------|
| | RS | TS | CTS |
| 0 | 227 (±6) | 251 (±14) | 221 (±9) |
| 5 | 291 (±6) | 278 (±14) | 269 (±12) |
| 10 | 302 (±8) | 288 (±8) | 289 (±8) |
| 15 | 321 (±13) | 355 (±17) | 332 (±10) |
| 20 | 335 (±18) | 325 (±13) | 329 (±13) |
| 25 | 344 (±11) | 361 (±7) | 352 (±11) |

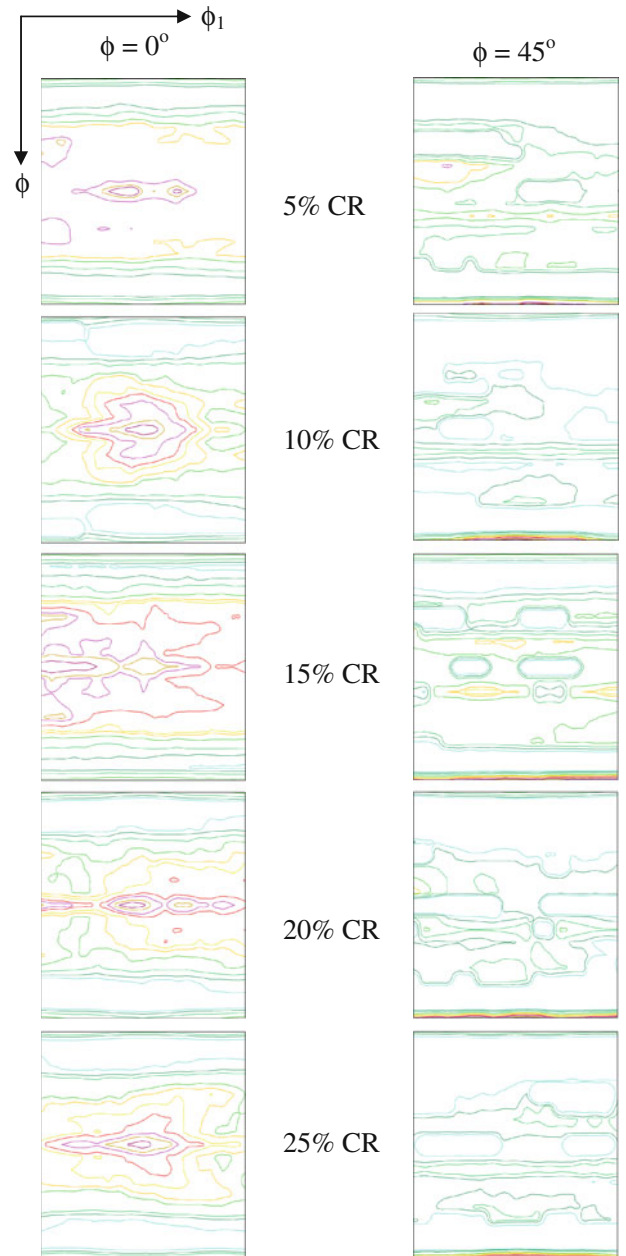


Fig. 10—ODFs on the outer rolling surface of stainless steels cold rolling from 5 to 25 pct.

increase was obtained by an initial 5 pct deformation. This also indicates that the rate of dislocations introduced by the initial 5 pct deformation is more than that at above 5 pct. The changes observed in the DIM were insignificant, and therefore, its role in increasing the hardness or DOS might be similar at all deformations. In contrast, at a lower temperature such as 723 K (450 °C) for TS and CTS), deformations >5 pct accelerated the sensitization more rapidly than at <5 pct, which could be caused by the lower driving force or larger activation energy for sensitization at this temperature than at 773 K (500 °C) or higher. The lower driving force for sensitization <5 pct deformations at 723 K (450 °C) was overcome by increased deformations. The increase in DOS at 673 K (400 °C) was monotonous and seems far from saturation. The lower overall slope at this temperature indicates clearly the slow increase in sensitization kinetics as

compared to that at higher temperatures and thus is temperature dependent.

B. Sensitization on Orthogonal Surface

The degree of sensitization in deformed specimens has been determined and reported in the previous section, irrespective of the plane of the specimen subjected to the test. Consideration of the plane of measurement is important, particularly in a cold-rolled sheet, as several engineering properties are dependent on the surface with respect to the rolling direction (anisotropic) affected by changes in structural or physical properties of materials. It was noticed that the occurrence of sensitization on the three sections (RS, TS, and CTS) was almost of similar degree before deformation. A difference in the sensitization susceptibility among RS, TS, and CTS (Figures 1

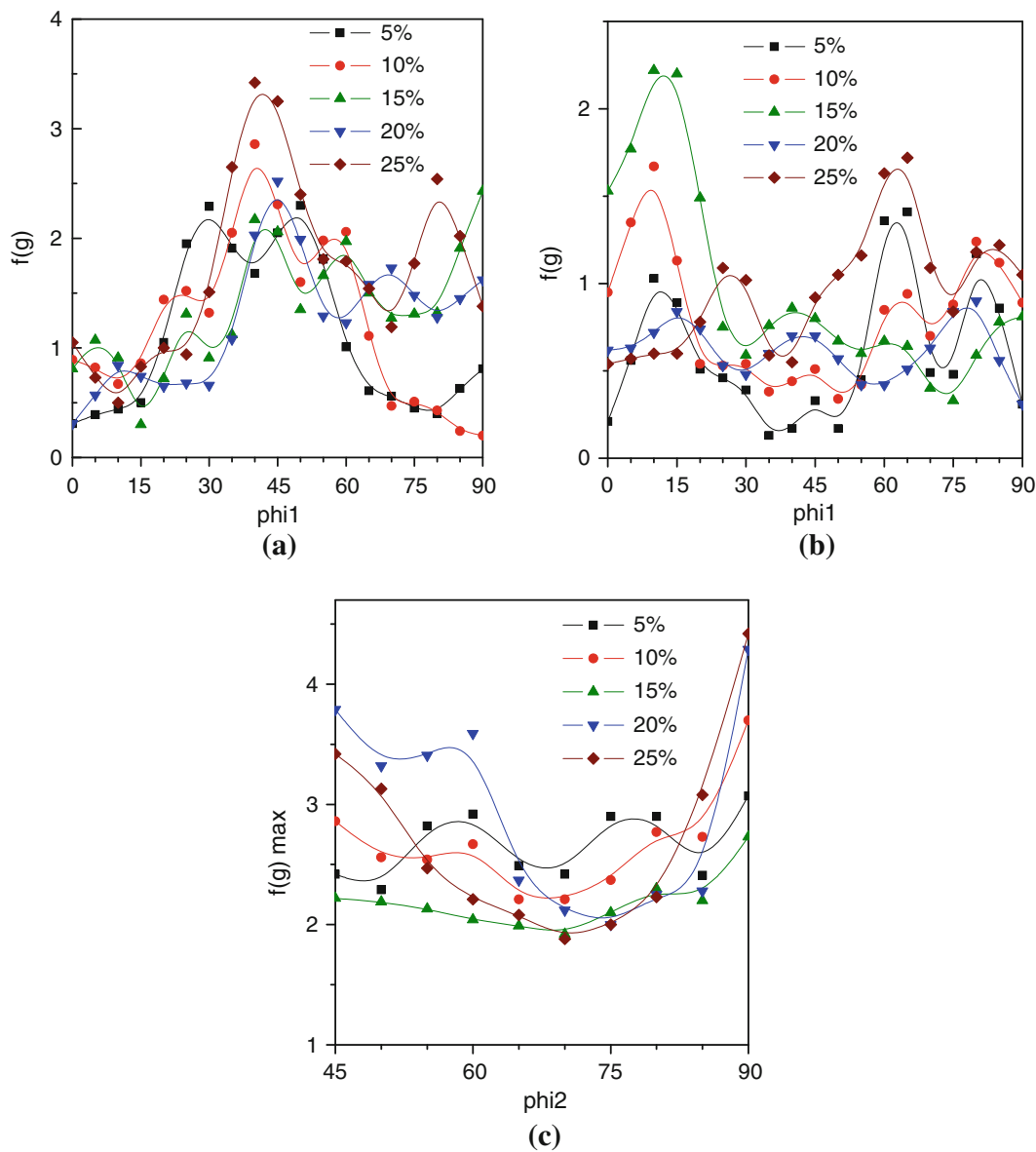


Fig. 11—Orientation density variation along (a) α -fiber, (b) τ -fiber, and (c) β -fiber on RS with percent cold rolling.

through 3) was observed after applying deformation. DOS was observed to be more pronounced on the CTS and TS compared with the RS. The DOS on the RS was generally lower (at 5 to 10 pct deformation) than that on the other two sections at all the studied temperatures.

A variation in DOS, among three surfaces, is expected because of a change in texture, percent martensite, dislocations, grain size, or any combination thereof. These changes in 304LN vis-à-vis DOS has been attempted and are elaborated in this section. The rolling texture was evaluated on the surface (on which DOS has been measured) as illustrated in Figure 10. In this figure, constant $\varphi_2 = 0$ and 45 deg sections are presented (rolling surface texture). After 5 pct cold rolling, rotated cube components and α -fiber orientations from brass to P are present. At 10 pct rolling, the texture is centered

mainly around the brass component, and there is no trace of a cube component. After 15 pct cold rolling, the texture is composed mainly of α -fiber orientations with a large scatter. At 20 pct, the evolution of texture remains same as that of 15 pct with less scatter. After 25 pct cold rolling, the main component is brass with a scatter toward goss.

To elucidate more on texture evolution on RS, fibers have been plotted and presented in Figure 11. Figure 11(a) shows an α -fiber plot with increasing cold rolling. It shows that at up to 10 pct cold rolling, the maxima lie around the brass position. With increasing cold reduction, there is an increase in the scatter around this position, and the scatter extends up to the rotated goss position. The τ -fiber plot (Figure 11(b)) shows the presence of a few components depending on the

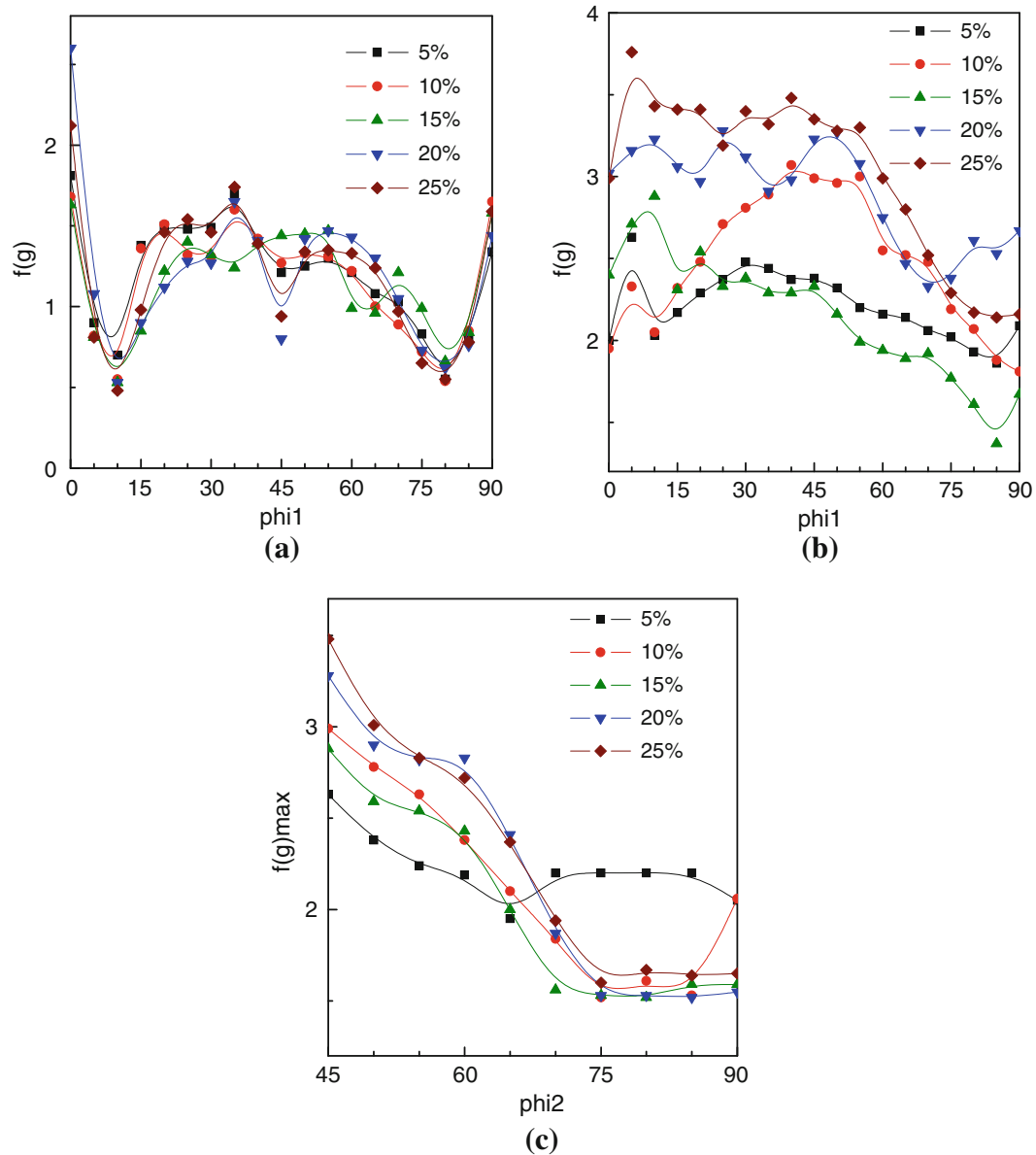


Fig. 12—Orientation density variation along (a) α -fiber, (b) τ -fiber, and (c) β -fiber on TS with percent cold rolling.

degree of rolling. Up to 10 pct cold rolling, there is a component near $\{110\}\langle 001\rangle$ as well as $\{332\}\langle 113\rangle$ at $\phi = 15$ deg. After 15 pct rolling, a component around $\phi = 15$ deg remains. At 20 pct rolling, no significant component can be observed, and the overall intensity of the fiber is weak. At 25 pct cold rolling, the major components are $\{332\}\langle 113\rangle$, $\{110\}\langle 001\rangle$, and a component at $\phi = 30$ deg. The β -fiber plots (Figure 11(c)) show nearly homogeneous evolution of all orientations along the fibers at the initial stages of rolling. With increasing rolling reduction, the main components are Cu $\{112\}\langle 111\rangle$ and brass $\{011\}\langle 211\rangle$.

Texture data for TS and CTS sections have been evaluated by appropriately rotating the texture evaluated for RS section. The fibers have been plotted from the texture data and are presented in this study. The

α -fiber plots for the TS section (Figure 12(a)) show mainly the presence of goss $\{011\}\langle 100\rangle$ and rotated goss $\{011\}\langle 011\rangle$ components. The τ -fiber plot (Figure 12(b)) shows $\{111\}\langle 112\rangle$ and $\{112\}\langle 111\rangle$ components. The β -fiber plot (Figure 12(c)) shows strong Cu $\{112\}\langle 111\rangle$ and S $\{123\}\langle 634\rangle$ with a weak brass component. Figure 13(a) shows the α -fiber plots on CTS section; it shows presence of goss and brass components along with weak rotated Goss component. The τ -fiber plot (Figure 13(b)) shows similar evolution with increasing rolling reduction with maxima at $\{001\}\langle 110\rangle$ and $\{110\}\langle 001\rangle$. The β -fiber (Figure 13(c)) shows also a similar evolution with increasing rolling reduction with stronger brass component compared with Cu and S components. After a close look on the evolution of texture and DOS after annealing at 673 K (400 °C)

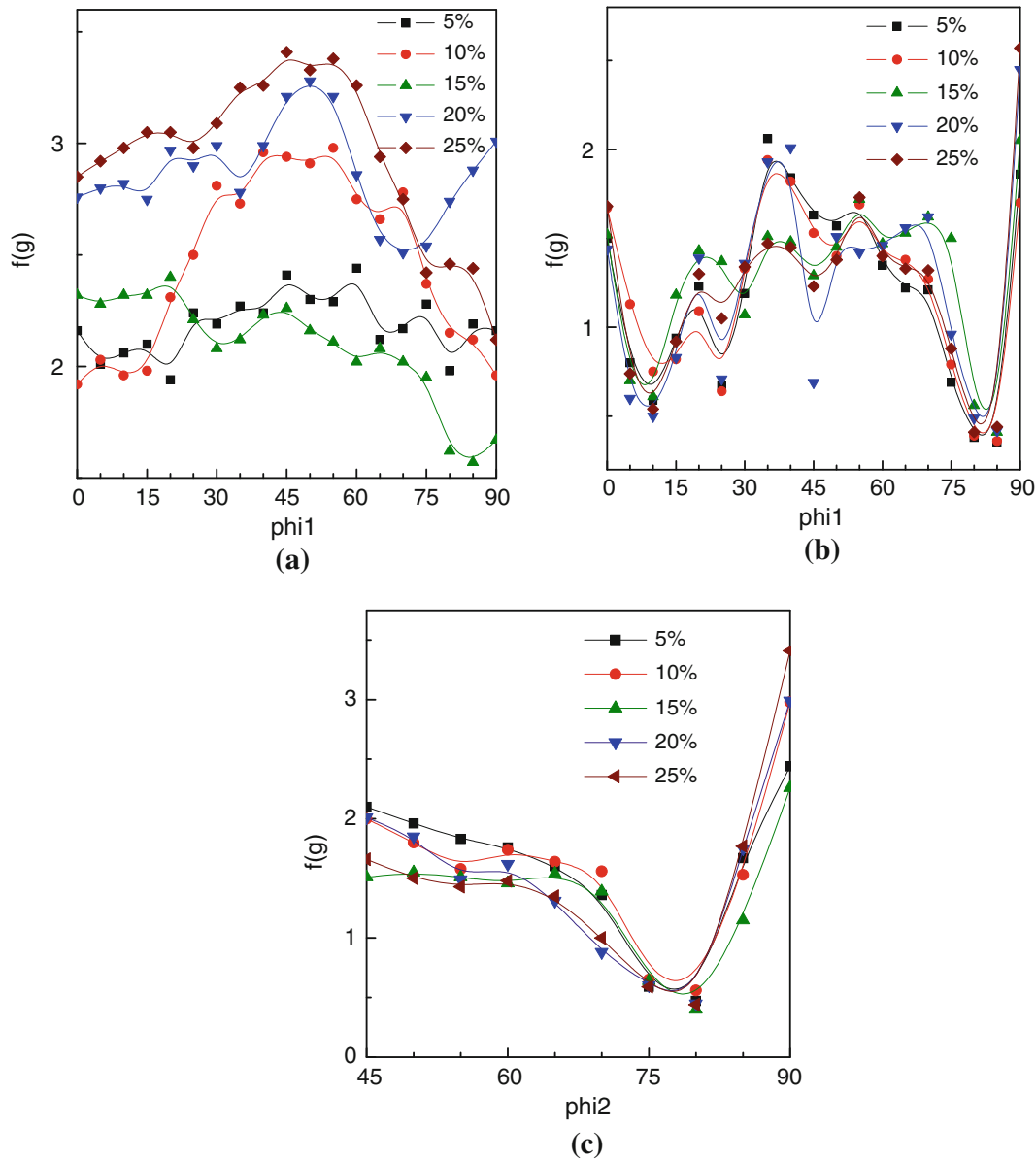


Fig. 13—Orientation density variation along (a) α -fiber, (b) τ -fiber, and (c) β -fiber on CTS with pct cold rolling.

(Figure 4 and Figures 11 through 13), it seems that the relation is not straightforward. In previous work on AISI316L, it has been observed that the components of rolling texture such as brass and Cu leads to lower DOS.^[23] With increase in annealing temperature, the difference in DOS among the three orthogonal orientations is going to decrease.

C. Microstructural Evolution on Orthogonal Surfaces

Thin foils were prepared from the orthogonal surfaces after different deformation conditions and examined under a transmission electron microscope (TEM). Two surfaces have been taken into account: RS and TS, where DOS shows significant difference. The samples cold rolled by 10 pct deformation show the cell structure at the rolling surface as illustrated in Figure 14(a). The TS section, however, shows the formation of stacking faults of smaller widths and lengths apart from cell structure within the microstructure (Figure 14(b)). After 25 pct cold rolling, the RS shows formation of shear bands (Figure 15(a)). At the intersection of shear bands, the formation of bcc-martensite was confirmed through selected area diffraction (SAD) pattern shown in Figure 15(b). Density of shear bands is more in TS

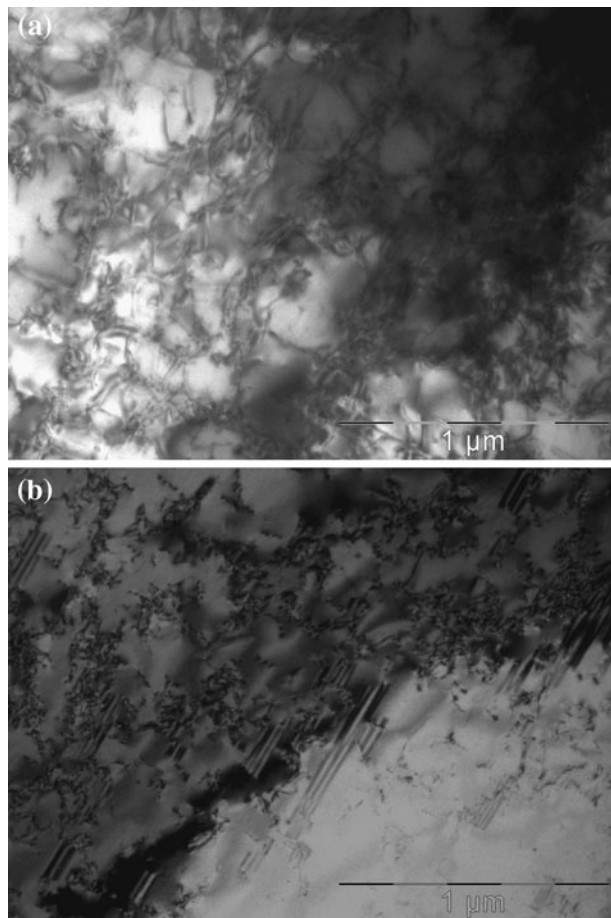


Fig. 14—TEM microstructure after 10 pct cold rolling: (a) rolling surface and (b) transverse surface.

(Figure 16(a)) than in RS deformed by 25 pct which could be one of the reasons of exhibiting higher DOS by the TS. Formation of bcc-martensite was confirmed in TS (Figure 16(a)). In some cases of TS, evidence of ϵ -martensite formation was seen (Figure 16(b)). Generally, austenite to martensite transformation proceeds as γ through ϵ to α as well as γ to α . Hence, the transformation in the present case proceeds through both the modes; however, mode of transformation depends on the texture.

IV. DISCUSSION

The DIM present on each surface is shown in Figure 9. DIM (by volume) was the highest along CTS (10 to 15 pct) followed by TS (3 to 6 pct), where the overall DOS was higher than on RS (1 to 3 pct). The change in the value of DIM with the increase in the degree of rolling was insignificant for the TS and RS sections, whereas for the CTS section, the increase in the DIM with a large scatter was noticed after 10 pct cold rolling. The difference in the volume fraction of DIM may be caused by a variation in the crystallographic texture of three orthogonal surfaces. Langeborg^[24] suggested that as the austenite-to-martensite transformation is stress or strain assisted, the transformation is orientation dependent. Also, the austenite and martensite have a well-defined crystallographic relationship with respect to each other.^[25,26] Experimental work carried out by Goodchild *et al.*^[27] shows that ϵ forms on the $\{111\}$ planes of γ grains preferably when the tensile stress is applied parallel to $\langle 110 \rangle$, whereas no transformation occurs with the stress applied in $\langle 100 \rangle$ direction. During the rolling, texture evolution, and phase transformation both take place simultaneously. Texture may cause an anisotropic transformation and the new phases also modify the initial texture of parent phase. Hence, the difference in martensite volume fraction may be related to the differential texture in the orthogonal sections of the samples.

In case of RS and TS, the austenite texture components are mainly Cu and brass as well as goss, Cu, S and $\{111\}$ components, respectively. The Cu:brass is nearly 1 in RS, whereas in TS, the brass component is negligible. In CTS, the main texture components are goss, brass, and $\{111\}$ components. Here, the ratio of Cu:brass is less than 1. It can, thus, be postulated that a ratio of brass:Cu equaling to 1 in the austenite phase is beneficial for the resistance to sensitization. It can be pointed out that $\{111\}_\gamma$ is parallel to $\{110\}_\alpha$ according to K-S orientation relationship. Brass texture corresponds to $\{011\}\langle 112 \rangle$, whereas the Cu texture corresponds to $\{112\}\langle 111 \rangle$. The difference with $\{111\}_\gamma$, which is one of the invariant plane for austenite with martensite, is larger for the brass texture, which leads to a lower fraction of the martensite phase during cold rolling. In the case of the TS section, in the absence of a brass component, the goss component $\{011\}\langle 100 \rangle$ is also unfavorable for martensite transformation. In the case of the CTS section, in α -fiber, one orientation lies at a higher ϕ_1 from the brass component. This section shows more martensite compared with the other two sections.

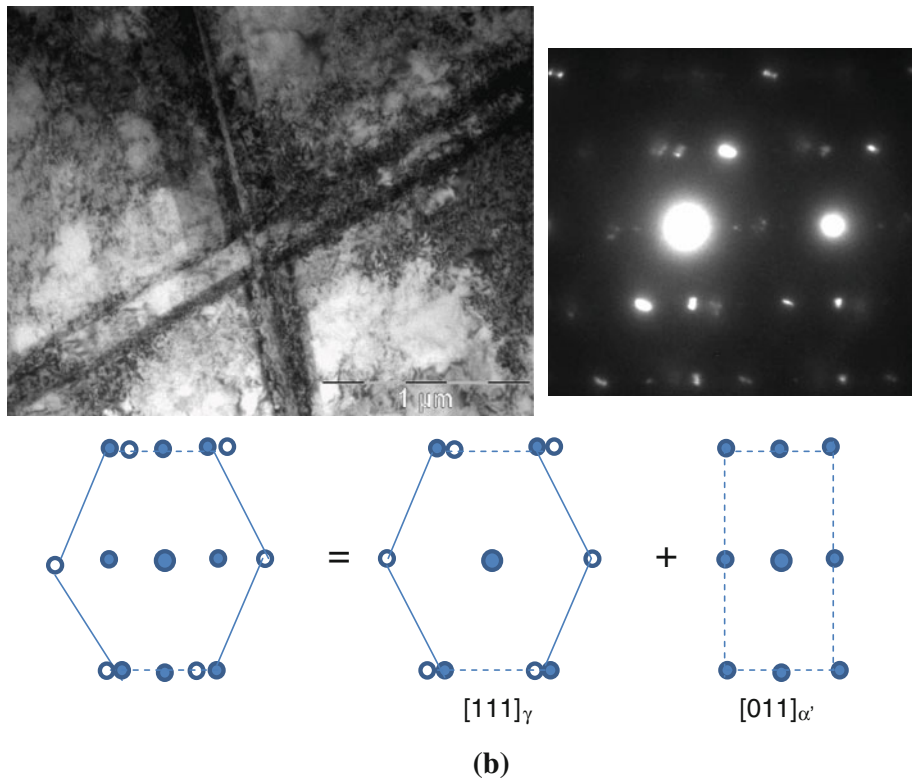
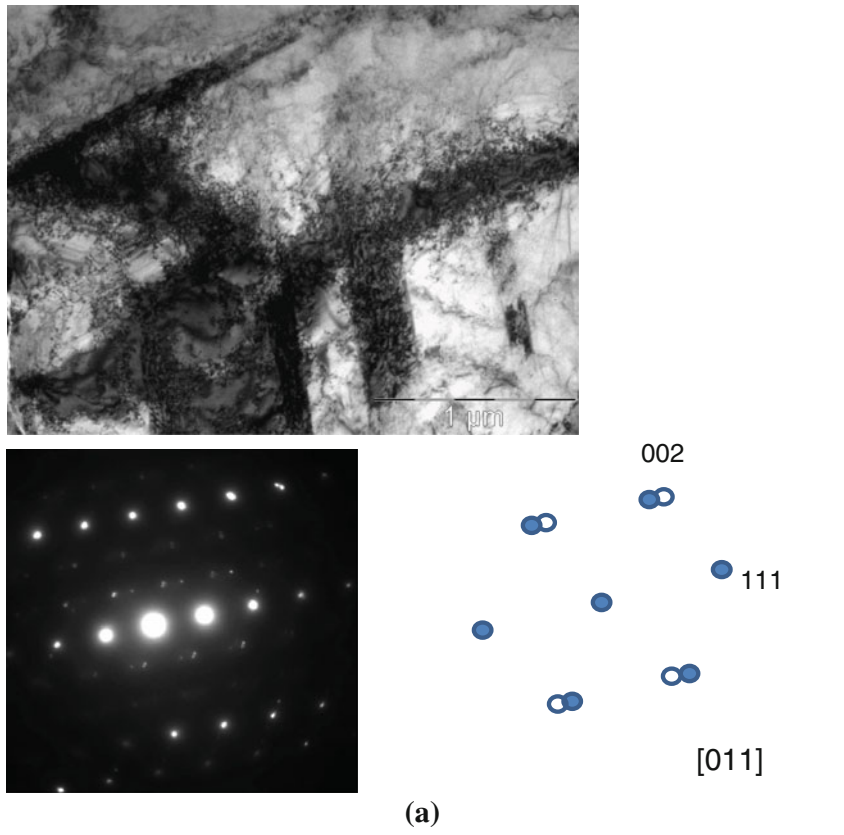


Fig. 15—TEM microstructure after 25 pct cold rolling: (a) showing shear bands and (b) intersection showing bcc martensite and SAD patterns on RS.

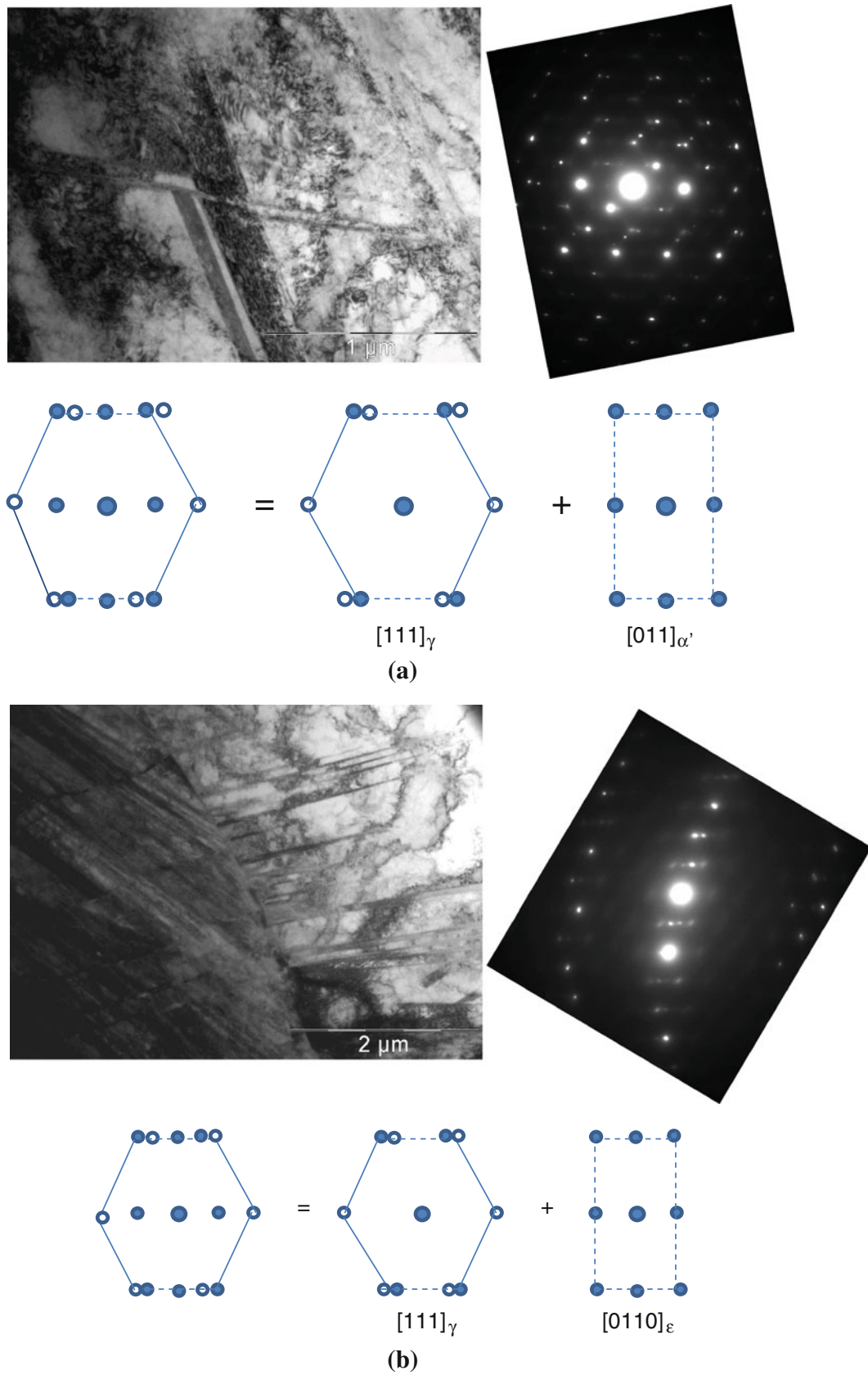


Fig. 16—TEM microstructure after 25 pct cold rolling: (a) shear bands and bcc martensite and (b) intersection showing ϵ martensite and SAD pattern on TS.

One important observation was a hike in the martensite volume fraction after 15 pct cold rolling. It might be observed that at 15 pct cold reduction, the α -fiber is weak and homogeneous; the β -fiber shows Cu:brass close to 1. Hence, the presence of the goss texture seems to be related with the higher martensite content. In addition, a component away from brass to higher ϕ_1 in the CTS section leads to more martensite formation; however, the exact cause for this is not clear at this stage.

In the DOS vs cold-rolling plot (Figure 4), it can be observed that the percent DOS is lower at 673 K (400 °C), whereas above this temperature, the percent DOS is higher. At 723 K (450 °C), it is nearly double to that observed at 673 K (400 °C). At temperatures 773 K (500 °C) and 873 K (600 °C), the nature of variation of DOS is similar with respect to the degree of cold rolling. At these temperatures, *i.e.*, 773 K to 873 K (500 °C to 600 °C), the percent DOS increases drastically after 5 pct cold rolling and reaches near saturation with a subsequent increase in cold reduction. The susceptibility to sensitization (percent DOS) differs significantly among orthogonal surfaces, particularly between RS and CTS/TS, at 673 K (400 °C) and 723 K (450 °C) unlike at relatively higher temperatures. The difference in the percent DOS is not much between CTS and TS sections, even though the former has a higher amount of DIM. It might be pointed out that during deformation, the stored energy gets reduced because of formation of martensite. In that context, the driving force or the amount of defects will be higher in the case of TS and RS compared with CTS. It has been reported that the activation energy of chromium carbide precipitation in martensite containing stainless steel is much less (<55 Kcal/mol) than that of pure austenite phase (100 to 150 Kcal/mol) at temperature <723 K (450 °C). Therefore, the DOS seems to be influenced by two factors: martensite fraction and the defect density. In case of CTS, martensite fraction is higher, whereas the density of defects is lower. In the case of TS, the martensite fraction is lower, whereas the defect density is higher. Hence, DOS in CTS and TS sections is balanced by both martensite fractions and defect density.

However, the anomaly with respect to the preceding arguments does not fit to the RS section. It shows a martensite fraction similar to TS but resulted in lower DOS at temperatures below 723 K (450 °C). The reason could be that the area selected for the DOS measurements is the outermost surface (RS), which had uniform deformation. Being in the direct contact of rollers, the outermost surface (skin) is expected to contain a greater defect density and more dislocation/slip band formation. This is supported by the increase in hardness from 227 to 344 HV_{100g} of 0 to 25 pct rolled specimens on the RS. Thus, because of larger defect density, the RS contains a high density of chromium-depleted zones with a restricted drop in chromium to below ~12 pct from adjacent regions that is detectable by DL-EPR test. As a result, the RS resulted in a lower DOS compared with CTS and TS. It may be noted also here that deformations on CTS and TS may not be uniform, as strain reduces across the depth of the rolled specimen.

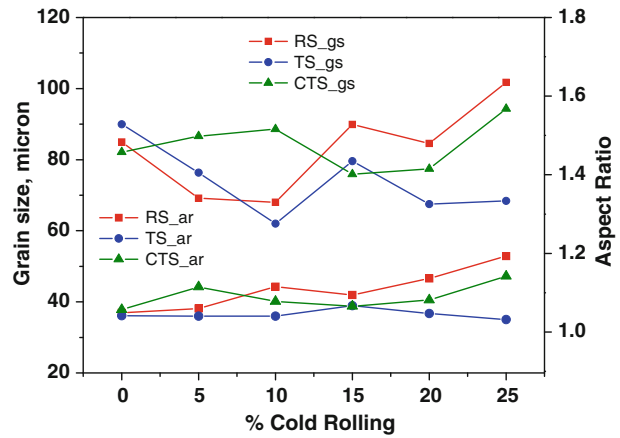


Fig. 17—Variation of grain size (gs) and aspect ratio (ar) with cold rolling.

The grain size and aspect ratio (major to minor axis) of various cold-rolled specimens on the three orthogonal surfaces have also been measured and are plotted in Figure 17. It indicates only a slight change in the grain structure with increasing percent rolling. Both the grain size and the aspect ratio have been observed to decrease with an increase in cold rolling up to 10 pct for RS and CTS; after that, they increase with percent cold rolling. For TS, the aspect ratio remains nearly the same, whereas the grain size decreases with percent cold rolling. Such changes in the grain size and aspect ratio on the DOS, however, might be overshadowed by the deformation effect. It was shown in our previous findings that the DOS (primarily because of grain boundary chromium depletion) increases with grain sizes in the strain-free state and vice versa.^[28] Such relationships are not applicable, in the current situation, because of the presence of a second phase (martensite) and defects/slip bands, which create diffusion short cuts.

V. CONCLUSIONS

Sensitization in prior deformed specimens occurred even at a low temperature ~673 K (400 °C). The variation of the degree of sensitization was observed among orthogonal surfaces of AISI 304LN, which were deformed prior to aging. The RS showed a lower DOS compared with CTS and TS. The differences in the DOS were attributed to the combined effect of DIM, grain size, and slip band formation, and the DOS widened with an increase in deformation. A deformation of 5 pct was critical to the susceptibility of AISI 304LN to IGC and transgranular corrosion. The sensitization kinetics slowed down beyond 5 pct deformations at 773 K (500 °C) and 873 K (600 °C). It was, however, uniformly accelerated over 5–25 pct deformation when aged at 673 K (400 °C). In terms of textures, the brass component is better for lower DOS; whereas the goss component has inverse behavior leading to higher DOS. It has been observed that the ratio of brass to copper should have a critical value for lower DOS, whereas an increase in the ratio will lead to poor DOS.

ACKNOWLEDGMENTS

The authors thank the Board of Research in Nuclear Science (BRNS) for funding this work (Grant GAP-0172). Help rendered by Shri Mukesh Kumar and Ujjwal Mukherji during experimental work is acknowledged gratefully.

REFERENCES

1. M.J. Povich: *Corrosion*, 1978, vol. 34, pp. 60–65.
2. M.J. Povich and P. Rao: *Corrosion*, 1978, vol. 34, pp. 269–75.
3. T. Kekkonen, P. Aaltonen, and H. Hanninen: *Corros. Sci.*, 1985, vol. 25, pp. 821–38.
4. T.A. Mozhi, M.C. Juhas, and B.E. Wilde: *Scripta Metall.*, 1987, vol. 21, pp. 1547–52.
5. S.M. Bruemmer, L.A. Charlott, and B.W. Arey: *Corrosion*, 1988, vol. 44, pp. 328–33.
6. R. Beltran, J.G. Maldonado, L.E. Murr, and W.W. Fisher: *Acta Mater.*, 1997, vol. 45, pp. 4351–60.
7. S. Pednekar and S. Smialowska: *Corrosion*, 1980, vol. 36, pp. 565–77.
8. R.L. Fullman: Electric Power Research Institute Report No. WS-79-17, 1980.
9. N. Parvathavarthini, R.K. Dayal, S.K. Sheshadri, and J.B. Gnanamoorthy: *J. Nucl. Mater.*, 1989, vol. 168, pp. 83–96.
10. R. Singh, B.R. Kumar, A. Kumar, P.K. Dey, and I. Chatteraj: *Metall. Mater. Trans. A*, 2003A, vol. 35A, pp. 2441–47.
11. V. Kain, K. Chandra, K.N. Adhe, and P.K. De: *J. Nucl. Mater.*, 2004, vol. 334, pp. 115–32.
12. V. Kain, K. Chandra, K.N. Adhe, and P.K. De: *Corrosion*, 2005, vol. 61, pp. 587–93.
13. D.R. Askeland: *The Science and Engineering of Materials*, Chapman Hall, Oxford, UK, 1996, pp. 188–215.
14. R.K. Dayal, N. Parvathavarthini, J.B. Gnanamoorthy, and P. Rodriguez: *Proceeding: Stainless Steel Processing and Metallurgy*, P.K. Rao, M.K. Asundi, N.B. Ballal, and S. Gadiyar, eds., 1992, pp. 385–91.
15. R. Singh, G. Das, P.K. Singh, and I. Chatteraj: *Metall. Mater. Trans. A*, 2009, vol. 40A, pp. 1219–34.
16. ASTM Standard Designation A262-Practice A-F, 1994, ASTM, Philadelphia, PA, 1993, vol. 03.02, pp. 1–16.
17. P. Umemura, M. Akashi, and T. Kawamoto: *Corros. Eng.*, 1980, vol. 29, pp. 163–68.
18. N. Saito, Y. Tsuchiya, F. Kano, and N. Tanaka: *Corrosion*, 2000, vol. 56, pp. 57–69.
19. E. Almanza and L.E. Murr: *J. Mater. Sci.*, 2000, vol. 35, pp. 3181–88.
20. L.E. Murr and F.I. Grace: *Trans. TMS-AIME*, 1969, vol. 245, pp. 2225–35.
21. A.F. Padilha, R.L. Plaut, and P.R. Rios: *ISIJ Int.*, 2003, vol. 43, pp. 135–43.
22. L.F.M. Martins, R.L. Plaut, and A.F. Padilha: *ISIJ Int.*, 1998, vol. 38, pp. 572–79.
23. S.G. Chowdhury and R. Singh: *Scripta Mater.*, 2008, vol. 58, pp. 1102–05.
24. R. Langeborg: *Acta Metall.*, 1964, vol. 12, pp. 823–43.
25. J.F. Breedis and W.D. Robertson: *Acta Metall.*, 1962, vol. 11, pp. 1077–88.
26. D.A. Porter and K.E. Easterling: *Phase Transformation in Metals and Alloys*, Chapman & Hall, London, UK, 1992, pp. 401–06.
27. D. Goodchild, W.T. Roberts, and D.V. Wilson: *Acta Metall.*, 1970, vol. 18, pp. 1137–45.
28. R. Singh, S.G. Chowdhury, B. Ravi Kumar, S.K. Das, P.K. De, and I. Chatteraj: *Scripta Mater.*, 2007, vol. 57, pp. 185–88.